

SCIENTIFIC REPORTS



OPEN

Microbial biotransformation of DON: molecular basis for reduced toxicity

Received: 04 April 2016

Accepted: 14 June 2016

Published: 06 July 2016

Alix Pierron^{1,2,3,*}, Sabria Mimoun^{1,2,*}, Leticia S. Murate^{1,4}, Nicolas Loiseau^{1,2}, Yannick Lippi^{1,2}, Ana-Paula F. L. Bracarense⁴, Gerd Schatzmayr³, Jian Wei He⁵, Ting Zhou⁵, Wulf-Dieter Moll³ & Isabelle P. Oswald^{1,2}

Bacteria are able to de-epoxidize or epimerize deoxynivalenol (DON), a mycotoxin, to deepoxy-deoxynivalenol (deepoxy-DON or DOM-1) or 3-epi-deoxynivalenol (3-epi-DON), respectively. Using different approaches, the intestinal toxicity of 3 molecules was compared and the molecular basis for the reduced toxicity investigated. In human intestinal epithelial cells, deepoxy-DON and 3-epi-DON were not cytotoxic, did not change the oxygen consumption or impair the barrier function. In intestinal explants, exposure for 4 hours to 10 μ M DON induced intestinal lesions not seen in explants treated with deepoxy-DON and 3-epi-DON. A pan-genomic transcriptomic analysis was performed on intestinal explants. 747 probes, representing 323 genes, were differentially expressed, between DON-treated and control explants. By contrast, no differentially expressed genes were observed between control, deepoxy-DON and 3-epi-DON treated explants. Both DON and its biotransformation products were able to fit into the pockets of the A-site of the ribosome peptidyl transferase center. DON forms three hydrogen bonds with the A site and activates MAPKs (mitogen-activated protein kinases). By contrast deepoxy-DON and 3-epi-DON only form two hydrogen bonds and do not activate MAPKs. Our data demonstrate that bacterial de-epoxidation or epimerization of DON altered their interaction with the ribosome, leading to an absence of MAPK activation and a reduced toxicity.

Mycotoxins are toxic secondary metabolites produced by various molds, such as *Aspergillus*, *Penicillium* and *Fusarium* which may contaminate food and feed at all stages of the food/feed chain^{1,2}. Despite the improvement of agricultural and manufacturing practices, mycotoxin contamination cannot be avoided and still represents a permanent health risk for both humans and animals. It is thus important to develop decontamination strategies³. Among mycotoxins, deoxynivalenol (DON) produced by *Fusarium* species, is commonly detected in cereal crops, including wheat, barley, and maize. It is the most abundant trichothecene in food with a frequent occurrence at toxicologically relevant concentrations worldwide^{4,5}.

DON causes acute and chronic disorders in humans and animals, with the gastrointestinal tract being an organ sensitive to its adverse effects⁶. DON affects the intestinal histomorphology, impairs barrier function and nutrient absorption^{7,8}. DON also disrupts the local intestinal immune response; it triggers and potentiates intestinal inflammation^{9,10}. At the cellular and subcellular level, DON binds to the ribosome, inhibits protein and nucleic acid synthesis and triggers ribotoxic stress^{11–13} leading to the activation of kinases, MAPKs and their downstream signaling pathways¹⁴.

Several strategies have been developed to limit DON toxicity¹⁵, among them, bacterial biotransformation which depends on the ability of microorganisms to generate DON metabolites with reduced toxicity. De-epoxidation is a reductive chemical reaction opening the 12,13-epoxy ring transforming DON into its de-epoxide metabolite deepoxy-deoxynivalenol (deepoxy-DON or DOM-1) (Supplementary Figure S1)¹⁶. Several microbial strains are capable of DON de-epoxidation^{15,17}. Several *in vitro* studies demonstrated the reduced toxicity of deepoxy-DON. *In vivo* trials on farm animals receiving feed contaminated with DON have

¹Toxalim, Research Center in Food Toxicology, Université de Toulouse, INRA, UMR 1331, ENVT, INP-Purpan Toulouse, France. ²Université de Toulouse, INP, UMR 1331, Toxalim, Toulouse, France. ³BIOMIN Research Center Technopark 1, 3430 Tulln, Austria. ⁴Universidade Estadual de Londrina, Lab. Patologia Animal, CP 6001, Londrina, Paraná, Brazil. ⁵Guelph Food Research Center Agriculture & Agri-Food Canada, Guelph, Ontario N1G 5C, Canada. *These authors contributed equally to this work. Correspondence and requests for materials should be addressed to I.P.O. (email: Isabelle.Oswald@toulouse.inra.fr)

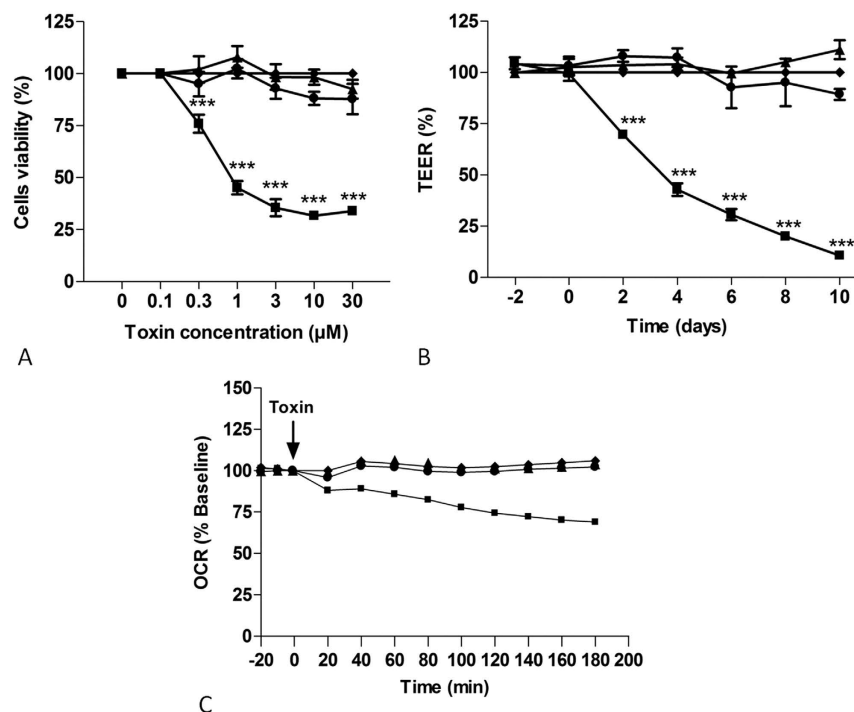


Figure 1. Effects of deepoxy-DON or 3-epi-DON on human intestinal epithelial cells. Activation of cytotoxicity (Panel A), TEER (Panel B) and OCR (Panel C). (Panel A): Proliferative Caco-2 cells were incubated with increasing concentrations of diluent (◆), DON (■), deepoxy-DON (▲) or 3-epi-DON (●) for 48 hours. Cell viability evaluated by measurement of ATP, is expressed as % of control cells. (Panel B): Caco-2 cells, differentiated on inserts, were treated with 10 µM of diluent (◆), DON (■), deepoxy-DON (▲) or 3-epi-DON (●) and TEER was measured. (Panel C): After establishment of baseline oxygen consumption rate in proliferated Caco-2 cells seeded to 1.5×10^4 cells/well, diluent (◆), DON (■), deepoxy-DON (▲) or 3-epi-DON (●), was injected at final concentration of 10 µM as indicated by the arrow. The rate of oxygen consumption was then measured for the indicated time. For visual clarity, statistical indicators were omitted from the graph. The OCR values are shown as the percent of baseline for each group. Results are expressed as mean \pm SEM of 3–4 independent experiments, *** $p < 0.001$.

also shown a beneficial effect of the bacteria able to de-epoxidize DON, according to zootechnical parameters and immune response¹⁸. The hydroxyl on carbon 3 also seems to be significant for the toxic activity of DON and a detoxification strategy targeting this part of the C3-OH, leading to the formation of 3-epi-DON, was recently proposed¹⁹. Four bacterial strains, all isolated from soil, have been described to epimerize DON into 3-epi-DON^{20,21}. Only one paper has investigated the effect of 3-epi-DON and demonstrated the lack of toxicity, both *in vitro* and *in vivo*, of this DON metabolite²².

The aim of the current study was to assess the efficacy of microbial transformation through analysis of the intestinal toxicity of deepoxy-DON and 3-epi-DON. Using physiological, histological and transcriptomic analysis, we have observed reduced toxicity of deepoxy-DON and 3-epi-DON, both for human intestinal epithelial cells and pig intestinal explants. We have further demonstrated that these microbial metabolites of DON fit into the ribosome pocket but do not elicit ribotoxic stress or activate the MAPKinase pathway. Our paper provides the first molecular insight for the reduced toxicity of deepoxy-DON and 3-epi-DON.

Results

Deepoxy-DON and 3-epi-DON do not impair proliferation of human intestinal cells.

Comparative effects of deepoxy-DON, 3-epi-DON and DON were first evaluated on proliferating human Caco-2 cells. The cell viability was assessed by the quantification of ATP using the luminescent cell viability assay. As shown in Fig. 1, Panel A, 48 hours exposure to deepoxy-DON or 3-epi-DON at concentrations up to 30 µM had no significant impact on cell viability. By contrast, DON markedly decreased the viability of proliferating cells in a dose-dependent manner; exposure to 10 µM of DON for 48 hours reduced cell viability by approximately 70%. The IC₅₀ was calculated at 1.30 µM.

Deepoxy-DON and 3-epi-DON do not impair cell viability and TEER of differentiated human intestinal cells.

The comparative toxicity of deepoxy-DON, 3-epi-DON and DON was also performed on differentiated Caco-2 cells through the measurement of TEER. As already described²³, differentiated cells are more resistant to DON and at least 30 µM are needed to induce a significant decrease in viability. At 10 µM of DON, a significant decrease of TEER in differentiated Caco-2 cells at a non-cytotoxic dose was observed (Fig. 1, Panel B).

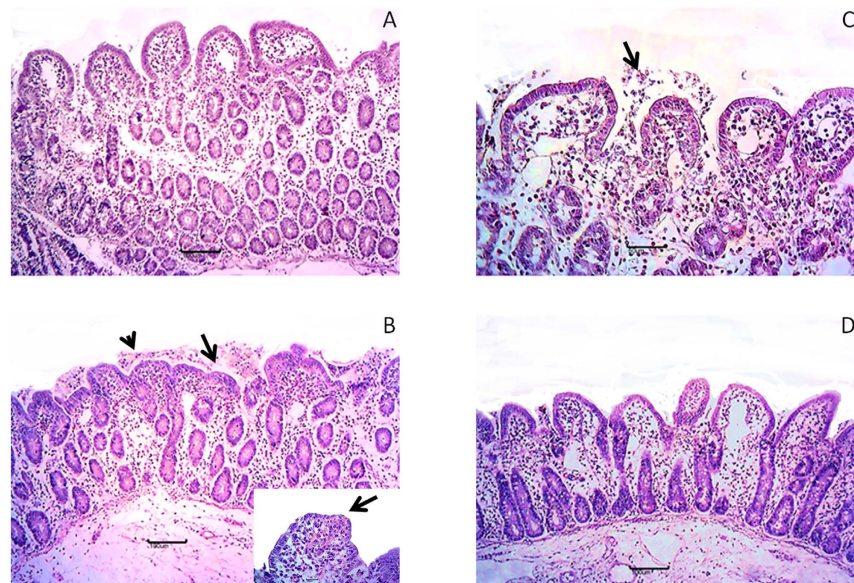


Figure 2. Comparative effects of deepoxy-DON and 3-epi-DON and DON on morphology of intestinal explants. Jejunal explants from 4 different animals were exposed for 4 hours, to diluent or 10 μ M toxins and stained with HE for histological analysis. Normal villi lined with columnar enterocytes were observed on control explants (Panel A) multifocal villi atrophy (arrow) and cell debris (arrowhead), apical necrosis (insert) on DON explants (Panel B) histological aspects similar to control group on deepoxy-DON (Panel C) or 3-epi-DON (Panel D) explants. Bar 100 μ m; insert bar 20 μ m.

The decrease was time-dependent and reached 25% after 2 days and about 90% at 10 days. By contrast, cells treated with 10 μ M deepoxy-DON or 3-epi-DON didn't show any decrease in TEER.

Deepoxy-DON and 3-epi-DON do not affect oxygen consumption in Caco-2 cells. The impact of deepoxy-DON, 3-epi-DON and DON on bioenergetic function in Caco-2 cells was evaluated using extracellular flux analyses. As shown in Fig. 1, Panel C, DON linearly decreased the rate of oxygen consumption in a time-dependent manner starting at the 40 minute stage. Approximately 3 hours after DON exposure, oxygen consumption values were 32% less than the base value. By contrast, deepoxy-DON and 3-epi-DON had no effect on the cellular oxygen consumption of proliferating Caco-2 cells and displayed bioenergetics profiles comparable to that of control cells.

Deepoxy-DON and 3-epi-DON do not induce histological alterations of intestinal explants. In order not to restrict the observations to an intestinal cell line, experiments were also performed on jejunal explants, a model developed to assess short-term effects of mycotoxins²⁴. The effects on intestines of deepoxy-DON, 3-epi-DON and DON were first compared with histology (Fig. 2). Lymphatic vessel dilation was observed at different intensities in all groups. Control explants displayed normal villi lined with columnar enterocytes (Fig. 2, Panel A). Explants exposed to deepoxy-DON (Fig. 2, Panel C) and 3-epi-DON (Fig. 2, Panel D) presented similar features but mild interstitial edema and cell debris on apical surface (arrow) were also observed. By contrast, multifocal to diffuse villi atrophy, multifocal villi fusion (arrows), necrosis of apical enterocytes and cellular debris (arrowhead, Fig. 2, Panel B) were observed after 4 hours of explant incubation with 10 μ M of DON.

Deepoxy-DON and 3-epi-DON do not induce intestinal inflammation. To complete the analysis of the intestinal toxicity of deepoxy-DON and 3-epi-DON, their effects on the expression of inflammatory genes were analyzed by RT-qPCR. As already described⁹, a strong intestinal inflammatory response was observed in jejunal explants in the presence of DON and a significant increase in expression of IL-1 α , TNFA, IL-1 β , IL-8, IL-12p40, IL-17A and IL-22 was also observed (Table 1). By contrast, no induction in the expression of these genes was observed in deepoxy-DON and 3-epi-DON treated explants, demonstrating that microbial transformation of DON to deepoxy-DON or 3-epi-DON led to decreased inflammatory response in intestinal explants (Table 1).

DON but not deepoxy-DON and 3-epi-DON changes gene expression profile in intestinal explants. The effects of DON, deepoxy-DON and 3-epi-DON were investigated beyond the inflammatory response, through a genome wide transcriptomic analysis. Exposure to DON resulted in differential expression of 747 probes; 681 and 66 probes corresponding to 303 and 33 genes were up- and down-regulated respectively (Fig. 3, Panel A). By contrast, no genes were differentially expressed in deepoxy-DON and 3-epi-DON treated explants when compared to control explants, indicating that microbial transformation of DON to deepoxy-DON or 3-epi-DON abolishes the toxicity of the mycotoxin.

DON differentially expressed genes were then selected to perform principal component analysis (PCA) (Fig. 3, Panel B) and cluster analysis (Fig. 3, Panel C). Two clusters were distinguished, indicating up-regulated

Cytokines	Explant treatments			
	Control	DON	Deepoxy-DON	3-epi-DON
<i>IL1B</i>	1.00 ± 0.40 ^a	17.4 ± 5.1 ^b	0.7 ± 0.2 ^a	0.8 ± 0.3 ^a
<i>IL1A</i>	1.00 ± 0.30 ^a	3.9 ± 1.4 ^b	0.9 ± 0.2 ^a	0.9 ± 0.2 ^a
<i>IL8</i>	1.00 ± 0.20 ^a	4.5 ± 1.2 ^b	1 ± 0.1 ^a	0.9 ± 0.2 ^a
<i>IL12p40</i>	1.00 ± 0.31 ^a	2.3 ± 0.4 ^b	1.2 ± 0.2 ^a	0.9 ± 0.2 ^a
<i>IL17A</i>	1.00 ± 0.50 ^a	15.8 ± 5.6 ^b	0.8 ± 0.1 ^a	1.3 ± 0.4 ^a
<i>IL22</i>	1.00 ± 0.30 ^a	7.9 ± 1.3 ^b	1.3 ± 0.5 ^a	1.4 ± 0.5 ^a
<i>TNFA</i>	1.00 ± 0.30 ^a	3.5 ± 0.5 ^b	1.1 ± 0.4 ^a	1.1 ± 0.3 ^a

Table 1. DON but not deepoxy-DON & 3-epi-DON up-regulated mRNA relative expression levels of pro-inflammatory cytokines and chemokines in pig jejunal explants. Notes: results are expressed in arbitrary units relative to control group. Results are mean ± SEM of 6 animals. Means in a row without a common letter differ (Newman-Keuls test, $P < 0.05$).

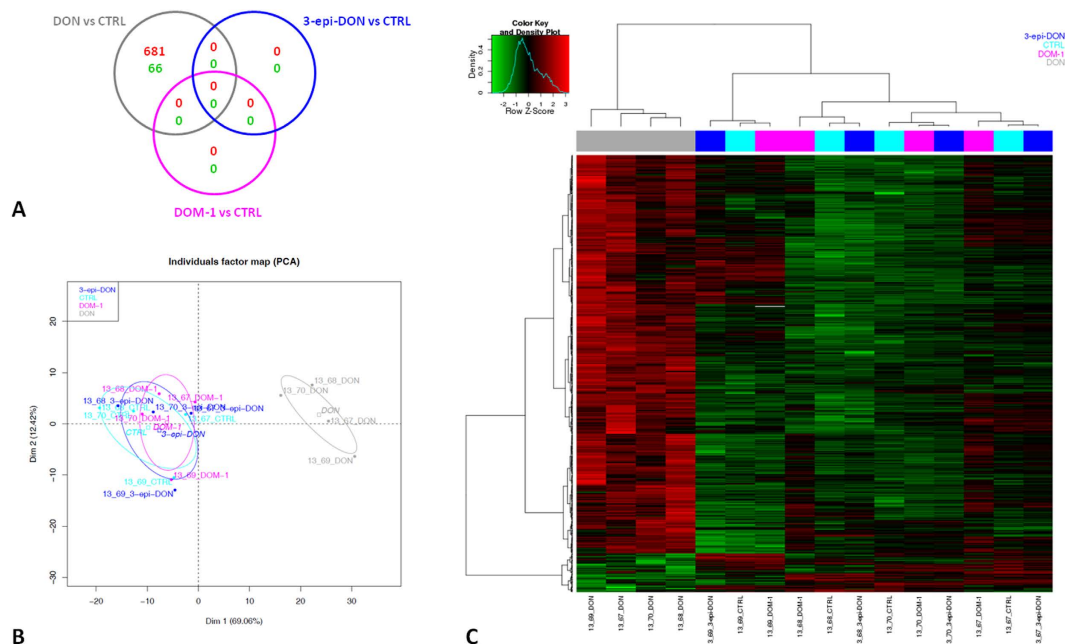


Figure 3. Gene expression profile of intestinal explants exposed to deepoxy-DON, 3-epi-DON or DON. Jejunal explants from 4 different animals were exposed for 4 hours, to diluent or 10 μ M toxins and gene expression was analyzed with a 60 K microarray. (Panel A): Venn diagram illustrating the overlaps between the probes significantly up- or down-regulated in response to DON, deepoxy-DON (DOM-1) and 3-epi-DON treatment. (Panel B): Principal Component Analysis of differentially expressed probes between DON, deepoxy-DON (DOM-1), 3-epi-DON and control (747 with BH adjusted p -value < 0.05). (Panel C): Heat map representing differentially expressed probes between DON, deepoxy-DON (DOM-1), 3-epi-DON and control explant. Red and green colors indicate values above and below the mean (average Z-score) respectively. Black color indicates values close to the mean.

and down-regulated genes (Supplementary Table S2). The most significantly up-regulated genes in DON-treated explants, with a change of more than 2.4 fold compared to control, were immune genes such as *CCL20*, *CXCL2*, *PRDM1*, *AREG*, *CSF2*, *FOSL1* (Table 2). As expected, the 6 pro-inflammatory cytokines already tested in RT-qPCR analysis were also up-regulated in the DNA array analysis; a strong correlation between the two methods of analysis was observed (coefficient $R^2 = 0.96$). DON also increased the expression of the ER heat shock protein HSP70 gene (*HSPA2*), genes of ubiquitination pathway (*HSPA2*, *BIRC2*, *NEDD4L*, *BIRC3*) and genes of metallothioneins (*MT1A*, *MT1M* and *MT2B*). DON decreased expression of the *CHAC1* gene, genes for molecular transport including *ABCC2*, *SLC15A1*, *SLC9A2*, the *CCL24* gene which is thought to play a role in the immune response, the *MLEC* gene which is connected to protein misfolding under conditions of endoplasmic reticulum (ER) stress, and other genes (Table 2).

Pathway analysis of differentially expressed genes exposed to DON was performed using Ingenuity Pathway Analysis software (IPA). The top 10 scored pathways are listed in Table 3, the entire list can be found as Supplementary Table S3. DON disturbed pathways related to immunity/inflammation, such as cytokines

Gene symbol	Gene name	−log (p-value)	Ratio
a. Up-regulated genes			
IL1B	interleukin 1 beta	4.428	1.29E-11
CCL20	chemokine (C-C motif) ligand 20	3.481	1.79E-06
IL1A	interleukin 1. alpha	3.207	6.46E-09
CXCL2	chemokine (C-X-C motif) ligand 2	3.129	1.87E-04
IL22	interleukin 22	2.955	1.13E-07
PRDM1	PR domain containing 1 with ZNF domain	2.793	4.76E-06
AREG/AREGB	amphiregulin	2.662	1.94E-11
CSF2	colony stimulating factor 2 (granulocyte-macrophage)	2.593	1.86E-05
IL8	interleukin 8	2.585	1.25E-06
FOSL1	FOS-like antigen 1	2.447	4.22E-04
IER3	immediate early response 3	2.446	1.95E-04
CCR7	chemokine (C-C motif) receptor 7	2.325	1.79E-08
CALCB	calcitonin-related polypeptide beta	2.313	9.03E-11
GADD45A	growth arrest and DNA-damage-inducible alpha	2.270	5.61E-08
TNFAIP3	tumor necrosis factor alpha-induced protein 3	2.260	1.36E-08
RND1	Rho family GTPase 1	2.255	3.24E-06
IER2	immediate early response 2	2.227	3.44E-06
CD83	CD83 molecule	2.207	1.10E-05
PLAUR	plasminogen activator. urokinase receptor	2.085	9.86E-04
BTG2	BTG family member 2	2.073	1.25E-06
IFRD1	interferon-related developmental regulator 1	2.025	1.14E-08
RGS1	regulator of G-protein signaling 1	2.020	3.24E-06
GEM	GTP binding protein overexpressed in skeletal muscle	2.013	4.52E-05
CCL4	chemokine (C-C motif) ligand 4	2.004	6.44E-04
STX11	syntaxin 11	1.989	4.27E-05
GADD45G	growth arrest and DNA-damage-inducible gamma	1.881	2.26E-06
GADD45B	growth arrest and DNA-damage-inducible beta	1.873	9.01E-04
NEDD9	neural precursor cell expressed developmentally down-regulated 9	1.870	1.15E-10
LAMA3	laminin. alpha 3	1.858	2.07E-05
CD274	CD274 molecule	1.846	8.75E-11
IL17A	interleukin 17A	1.844	2.11E-11
b. Down-regulated genes			
CHAC1	cation transport regulator homolog 1 (<i>E. coli</i>)	−1.696	9.18E-04
ABCC2	ATP-binding cassette sub-family C (CFTR/MRP) member 2	−1.015	2.45E-06
SLC15A1	solute carrier family 15 (oligopeptide transporter) member 1	−0.851	3.56E-05
SLC9A2	solute carrier family 9 subfamily A (NHE2 cation proton antiporter 2) member 2	−0.804	9.09E-06
CCL24	chemokine (C-C motif) ligand 24	−0.784	8.75E-04
MTTP	microsomal triglyceride transfer protein	−0.755	3.26E-05
DMBT1	deleted in malignant brain tumors 1	−0.666	2.67E-04
MLEC	Malectin	−0.654	9.50E-04
SSH1	slingshot protein phosphatase 1	−0.628	1.06E-03
VPS26B	vacuolar protein sorting 26 homolog B (<i>S. pombe</i>)	−0.610	1.04E-03
ACE2	angiotensin 1 converting enzyme 2	−0.607	7.35E-04
SCGB2A1	secretoglobin. family 2A member 1	−0.594	2.74E-04
MYEOV	myeloma overexpressed	−0.592	1.58E-04
NPR3	natriuretic peptide receptor 3	−0.582	8.74E-04
CBL	Cbl proto-oncogene. E3 ubiquitin protein ligase	−0.574	3.70E-04
PLOD2	procollagen-lysine 2-oxoglutarate 5-dioxygenase 2	−0.547	3.98E-05
C4BPA	complement component 4 binding protein Alpha	−0.525	1.04E-03
ARHGEF37	Rho guanine nucleotide exchange factor (GEF) 37	−0.521	9.19E-04
DESI2	desumoylating isopeptidase 2	−0.501	3.04E-04
STOML3	stomatin (EPB72)-like 3	−0.487	8.33E-04
Continued			

Gene symbol	Gene name	−log (p-value)	Ratio
UNC119B	unc-119 homolog B (<i>C. elegans</i>)	−0.467	2.42E-04
ZER1	zyg-11 related. cell cycle regulator	−0.455	4.92E-04
EGLN1	egl-9 family hypoxia-inducible factor 1	−0.443	2.26E-04
TCAP	titin-cap	−0.441	8.90E-04
PECAM1	platelet/endothelial cell adhesion molecule 1	−0.431	1.43E-04
ZCCHC14	zinc finger CCHC domain containing 14	−0.430	5.16E-04
GALNT4	polypeptide N-acetylgalactosaminyltransferase 4	−0.395	6.91E-04
ANKRD13A	ankyrin repeat domain 13A	−0.388	8.85E-04
UNC45A	unc-45 homolog A (<i>C. elegans</i>)	−0.377	7.64E-04
TPP1	tripeptidyl peptidase I	−0.375	5.37E-04
OSBPL7	oxysterol binding protein-like 7	−0.349	1.05E-03

Table 2. Top scored differentially expressed genes in DON treated porcine jejunal explants.

regulations (IL-17 axis, IL-10 signaling), leukocytes functions (diapedesis), iNOS and NFκB signaling. DON affected other pathways associated with cell cycle regulation, apoptosis and ER stress response. Moreover, the results underlined the effects of DON on PXR/RXR, FXR/RXR signaling pathways and mitochondrial L-carnitine Shuttle Pathways.

***In silico* analysis of the interaction of deepoxy-DON and 3-epi-DON with ribosomes and their inability to activate MAPKs.** The above data indicate that microbial transformation of DON into deepoxy-DON or 3-epi-DON abrogates its toxicity. The last step of this study was to investigate the underlying mechanism and more specifically to determine the ability of DON, deepoxy-DON and 3-epi-DON to bind to the A site of the ribosome peptidyl transferase center and to activate the MAPKs.

As expected, after 1 hour of exposure to 10 μM DON, MAPKs were activated in both differentiated monolayers Caco-2 cells and jejunal explants (Fig. 4). In cells, DON significantly increased phosphorylated p38 (3.24 ± 0.75 vs. 1 ± 0.09) compared to the control (relative intensity in arbitrary unit (A.U.); $p < 0.05$; $n = 3$) and phosphorylated SapKjunk (7.28 ± 0.64 vs. 1 ± 0.12 for control A.U.; $p < 0.05$; $n = 3$). By contrast, deepoxy-DON and 3-epi-DON were not able to activate these MAPKs in Caco-2 cells (Fig. 4 panel A). Similar trends were observed in jejunal explants (Fig. 4 panel B).

The last step was to investigate the ability of DON and its bacterial metabolites, deepoxy-DON and 3-epi-DON, to bind to the 60S subunit inside the A-site of the peptidyl transferase center of the ribosome. The crystallographic data (4U53.pdb) obtained for DON and yeast ribosomes were used¹³. As shown in Fig. 5, (panel A) DON is able to fit in the pocket of the A-site of the ribosome 60S subunit. Within the pocket, the 3-hydroxyl group of DON is associated with a magnesium atom and stabilized by other nucleotides. In this position, DON forms 3 hydrogen bonds with the A-site. The first one is between the oxygen of the DON epoxy group on C12 and one hydrogen of the sugar of the uracil U2873; the second one is between the oxygen of the C15 group CH₂OH and one hydrogen of the guanine basis G2403; and the last one is between the hydrogen of the C3 group and one oxygen of the uracil U2869. The *in silico* analysis revealed that both deepoxy-DON and 3-epi-DON were also able to fit into the pocket of the peptidyl transferase center of the ribosome (Fig. 5, Panel B and C). However, because of the absence of the epoxy group or the isomeric change, these two metabolites were only able to form 2 hydrogen bonds with the A sites of the peptidyl transferase center. Deepoxy-DON and 3-epi-DON did not form the bond with U2873 and U2869, respectively.

Discussion

Despite good agricultural practices, contamination by mycotoxins cannot be avoided. Several strategies have been developed to reduce mycotoxin exposure. Among them, microbial transformation is of interest but requires demonstration of the absence of toxicity of the metabolites produced. The aims of the present study were (i) to analyze the intestinal toxicity of two bacterial metabolites of DON, deepoxy-DON and 3-epi-DON and (ii) to investigate the molecular basis for their reduced toxicity.

Through the action of bacteria, DON can be epimerized on the hydroxyl group of C3 or de-epoxidized on the C12–C13 epoxide¹⁹. Epimerization is an aerobic irreversible transformation that may require two enzymatic activities of partially overlapping substrate specificity which occur together in sequence: oxidation of DON to 3-keto-DON and then conversion to 3-epi-DON. To date only four bacterial strains have been described to epimerize DON to 3-epi-DON¹⁹. A very recent paper shows that this bacterial metabolite is substantially less toxic than DON when tested *in vitro* on proliferating human Caco2 cells, as well as *in vivo* when given orally to mice for 14 days²². Deepoxy-DON is obtained after de-epoxidation of DON; several bacterial species and enzymes are able to catalyze this reaction¹⁹. The lower toxicity of deepoxy-DON, as compared to DON has been demonstrated *in vitro* on Swiss mouse 3T3 fibroblasts¹⁶, lymphocytes¹⁷ and brine shrimp²⁵. *In vivo* supplementation of DON-contaminated feed, with bacteria and/or an enzyme able to de-epoxidize DON, induced a reduction of the toxicity as shown by measurement of zootechnical or immune parameters^{18,26,27}.

In the present study, we observed reduced intestinal toxicity of 3-epi-DON and deepoxy-DON when compared to DON. The toxicity of DON and its bacterial metabolites was first investigated on proliferating and differentiated Caco-2 cells. As already demonstrated, DON induced a significant decrease in Caco-2 cell proliferation, reduced their barrier function and altered their respiratory capacities^{28–30}. This is the first investigation of the

Ingenuity Canonical Pathways	−log (p-value)	Ratio	Molecules
a. Up-regulated pathways			
Granulocyte Adhesion and Diapedesis	1.18E01	1.1E-01	<i>CCL3, IL1B, MMP12, EZR, CCL20, CLDN4, CCL3L1/CCL3L3, SELE, MMP13, CXCL2, VCAM1, CXCL8, CXCR4, IL18, IL1RN, TNF, CXCR2, ICCL4, XCL1</i>
Agranulocyte Adhesion and Diapedesis	1.13E01	1.04E-01	<i>CCL3, IL1B, MMP12, EZR, CCL20, CLDN4, CCL3L1/CCL3L3, SELE, MMP13, CXCL2, VCAM1, CXCL8, CXCR4, IL18, IL1RN, TNF, CXCR2, IL1A, CCL4, XCL1</i>
Glucocorticoid Receptor Signaling	1.11E01	7.69E-02	<i>HSPA2, NFKB1, CCL3, CSF2, JAK2, IL1B, PLA2, SELE, NFKBIE, NFATC1, NFKBIA, VCAM1, CXCL8, FOS, IL1RN, DUSP1, SGK1, NR3C1, TNF, SMAD3, CDKN1A, IL10, FOXO3</i>
Differential Regulation of Cytokine Production in Intestinal Epithelial Cells by IL-17A and IL-17F	1.07E01	3.91E-01	<i>CCL3, CSF2, IL1B, TNF, IL1A, IL17A, IL10, CCL4, IL17F</i>
Communication between Innate and Adaptive Immune Cells	1.01E01	1.25E-01	<i>CCR7, CCL3, CSF2, IL1B, CCL3L1/CCL3L3, CD40, CXCL8, CD83, IL18, IL1RN, TNF, IL1A, IL10, CCL4</i>
Differential Regulation of Cytokine Production in Macrophages and T Helper Cells by IL-17A and IL-17F	1.01E01	4.44E-01	<i>CCL3, CSF2, IL1B, TNF, IL17A, IL10, CCL4, IL17F</i>
Hepatic Fibrosis/Hepatic Stellate Cell Activation	9.55E00	1.03E-01	<i>CCR7, NFKB1, IL1B, EDNRB, MMP13, CD40, VCAM1, CXCL8, IFNGR1, TNF, SMAD3, IL1A, EDN1, IL4R, IL10, TIMP</i>
IL-10 Signaling	9.48E00	1.54E-01	<i>FOS, IL18, NFKB1, IL1RN, IL1B, SOCS3, TNF, IL1A, IL4R, IL10, NFKBIE, NFKBIA</i>
T Helper Cell Differentiation	9.41E00	1.67E-01	<i>GATA3, IFNGR1, BCL6, IL18, STAT4, TNF, ICOSLG/LOC102723996, IL17A, IL4R, IL10, CD40, IL17F</i>
Atherosclerosis Signaling	9.4E00	1.08E-01	<i>NFKB1, IL1B, SELE, MMP13, CD40, VCAM1, CXCL8, CXCR4, IL18, IL1RN, TNF, IL1A, F3, TNFRSF12A, PLA2G4A</i>
b. Down-regulated pathways			
PXR/RXR Activation	2.28E00	2.17E-02	<i>ABCC2, CPT1A</i>
FXR/RXR Activation	2.07E00	1.82E-02	<i>ABCC2, MTPP</i>
Mitochondrial L-carnitine Shuttle Pathway	1.57E00	4.55E-02	<i>CPT1A</i>
Granulocyte Adhesion and Diapedesis	1.49E00	1.1E-02	<i>CCL24, PECAM1</i>
Agranulocyte Adhesion and Diapedesis	1.44E00	1.04E-02	<i>CCL24, PECAM1</i>
LPS/IL-1 Mediated Inhibition of RXR Function	1.31E00	8.16E-03	<i>ABCC2, CPT1A</i>
Complement System	1.28E00	2.86E-02	<i>C4BPA</i>
Erythropoietin Signaling	9.87E-01	1.27E-02	<i>CBL</i>
Chemokine Signaling	9.75E-01	1.33E-02	<i>CCL24</i>
Ephrin B Signaling	9.46E-01	1.22E-02	<i>CBL</i>

Table 3. Ten top scored canonical pathways differentially regulated in 10 μ M DON treated porcine jejuna explants and list of genes in each pathway.

toxicity of deepoxy-DON on human intestinal epithelial cells, although the absence of toxicity of 3-epi-DON on Caco-2 cells has been recently demonstrated²².

The toxicity of DON and its bacterial metabolites on intestinal tissues was further evaluated. Because of the difficulties accessing human intestinal samples, the study was performed on porcine intestinal explants. Indeed, pigs are very sensitive to DON and can be considered good models for extrapolation to humans, with a digestive physiology very similar to that of humans^{8,31}. Histological assessment showed normal villi lined with columnar enterocytes, mild interstitial edema and cell debris on the apical surface for the control, 3-epi-DON and deepoxy-DON treated explants. This is in accordance with the absence of histopathological lesions observed in mice after a 14 day oral exposure to 25 or 100 mg 3-epi-DON/Kg bw (body weight)²². Effects of purified deepoxy-DON on the intestine have never been tested, however nutritional strategies including bacteria/enzyme transforming DON to deepoxy-DON have reduced the occurrence and extent of intestinal lesions¹⁸ and showed the same zootechnical performance as in control animals^{26,27}. By contrast, as already shown, treatment with 10 μ M of DON induces intestinal damage indicated by villi atrophy and villi fusion²⁴. To confirm that the two microbial transformation products of DON were not toxic, a pan-genomic analysis using a DNA array containing 62,976 probes was performed on jejunal explants. It revealed that no probes were differentially expressed between control explants and the ones treated with either deepoxy-DON or 3-epi-DON. To the best of our knowledge this is the first genome wide analysis performed for deepoxy-DON and 3-epi-DON.

The global transcriptomic analysis of the effect of DON on the intestine indicated that DON does not only interfere with genes involved in the immune response. As already described for human and murine thymus cells^{32–34}, DON exposure also targets ER (endoplasmic reticulum) stress, protein synthesis, oxidative stress, cell cycle regulation and apoptosis in intestinal tissues. The strong alteration of the gene *MLEC* implicated in misfolded glycoprotein quality control observed herein is likely due to the arrest of translation induced by ribotoxic stress. This leads to less protein entering the ER to temper the unfolded protein response and therefore protein synthesis³³. The increased gene expression of the ER heat shock protein HSP70 could also reduce the accumulation of unfolded protein in ER lumen. An increased expression of some genes involved in the ubiquitination pathway was observed in the presence of DON. This result could indicate that the presence of DON may induce the increase in proteins involved in protein degradation^{33,35,36}. Our data also underline the decrease of the unfolded protein response pro-apoptotic gene *CHAC1*. The *CHAC1* protein seems to play a role in glutathione degradation³⁷. ER stress could also induce leakage of calcium from the reticulum leading to activation of NFkB, NRF2-mediated oxidative stress response and apoptosis³³. The present work emphasizes the effect of DON on

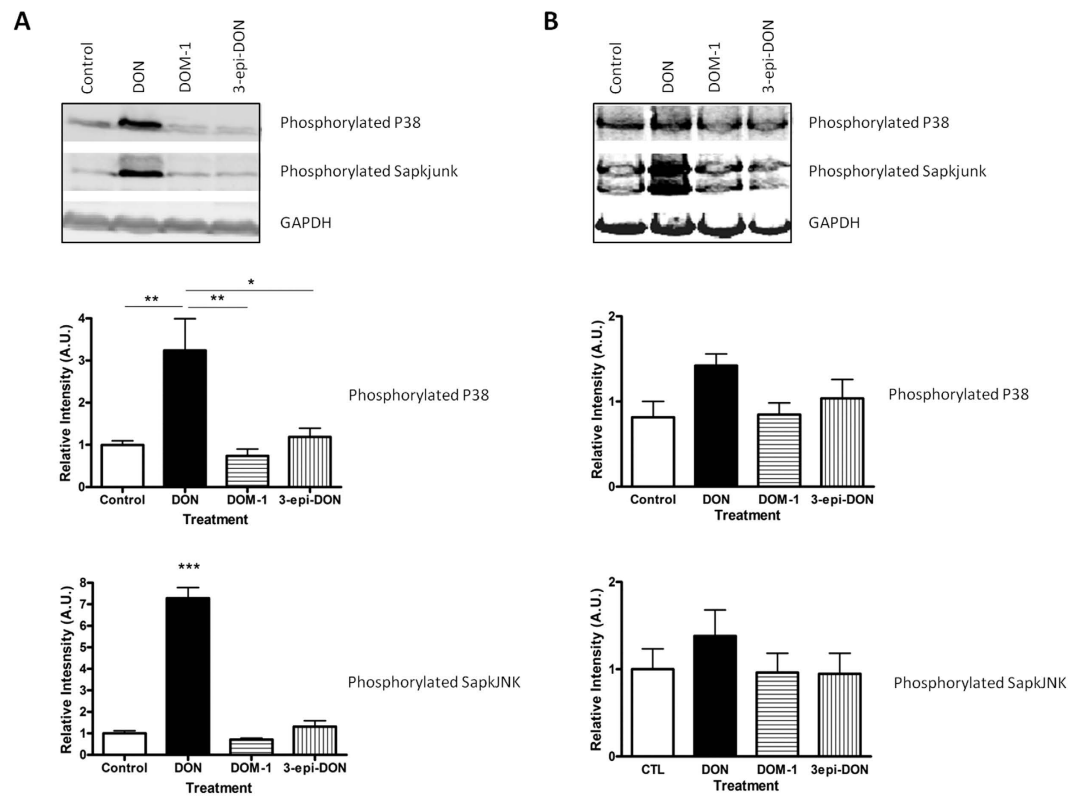


Figure 4. Effects of deepoxy-DON or 3-epi-DON on activation of MAPK on human intestinal epithelial cells. (Panel A): Caco-2 cells, differentiated on inserts. (Panel B): Jejunal explants. Samples were treated for 1 h with 10 μ M toxins and analyzed by western blot for expression of phosphorylated P38, phosphorylated JNK and GAPDH, used as a protein loading control. Representative immunoblots and normalized expression graph. Results are expressed as mean \pm SEM of 3–4 independent experiments, * $p < 0.05$, ** $p < 0.01$, *** $p < 0.001$.

metallothioneins MT1A, MT1M and MT2B. A relationship between metallothionein protein levels, used as a marker of oxidative stress, and mycotoxins in the liver of rats fed on naturally contaminated wheat has been reported³⁸. Therefore, it could be assumed that MTs are associated with pathways protecting the intestine against DON toxicity. The present study underlines the effect of DON on the genes of intestinal transporters. DON decreases the expression of the solute carrier *SLC15A1* and *SLC9A2* involved in proton-coupled oligopeptides transporter PepT1 and a Na⁺/H⁺ exchanger, respectively^{39,40}. Similar effects on other mRNA expression transporters as sugars transporters were described in the jejunum and to a lesser extent in the liver of broilers exposed to DON⁴¹. Accordingly, it has been experimentally shown that DON decreases the intestinal uptake of various nutrients in human epithelial intestinal cell line HT-29-D4⁴². This effect is likely due to a specific modulation of intestinal transporters expression, rather than a consequence of cell damage. The transcriptomic analysis demonstrates that DON down-regulates the expression of *ABCC2* gene that encodes for MRP2, a protein involved in efflux of DON and other mycotoxins and also in the transport of a wide range of organic anions including bile salt flow⁴³. An action of DON on mitochondrial dysfunction, attested to by the down-regulation of *CPT1A* mRNA was also observed in this study. *CPT1A* encodes for a key regulatory enzyme of β -oxidation and is required for transport of long chain fatty acids into mitochondria⁴⁴. The modulation of β -oxidation in addition to the modulation of intestinal transporters could explain the energy failure reported after DON exposure⁴². It is now necessary to investigate these changes at the protein level.

The use of bacteria is a promising approach to DON decontamination. In the present study we observed that deepoxy-DON and 3-epi-DON were devoid of intestinal toxicity. The underlying mechanism was further investigated. DON is known to develop its toxic potential by interacting with the peptidyl transferase at the 60S ribosomal subunit level, blocking the protein synthesis at the elongation step, inducing a ribotoxic stress and activating MAPKs^{7,12,13}. In accordance with literature, we observed that DON induced phosphorylation of JNK and p38 proteins^{24,45}. By contrast, deepoxy-DON and 3-epi-DON did not activate these signaling pathways, suggesting an absence of ribotoxic stress. To further the analysis, a modeling of deepoxy-DON and 3-epi-DON in the ribosome peptidyl transferase center was performed. DON and its bacterial metabolites fit into the A-site pocket, however whereas DON binds to the peptidyl transferase center with three hydrogen bonds, only two hydrogen bonds were identified between deepoxy-DON or 3-epi-DON and the peptidyl transferase center. This suggests that the absence of the epoxy group or the isomeric transformation decreases the affinity of these latter metabolites for the active site pocket A of the ribosome and prevents the induction of ribotoxic stress. *In silico* modeling revealed that a third hydrogen bond (the one between the oxygen of the C15 group CH2OH and the

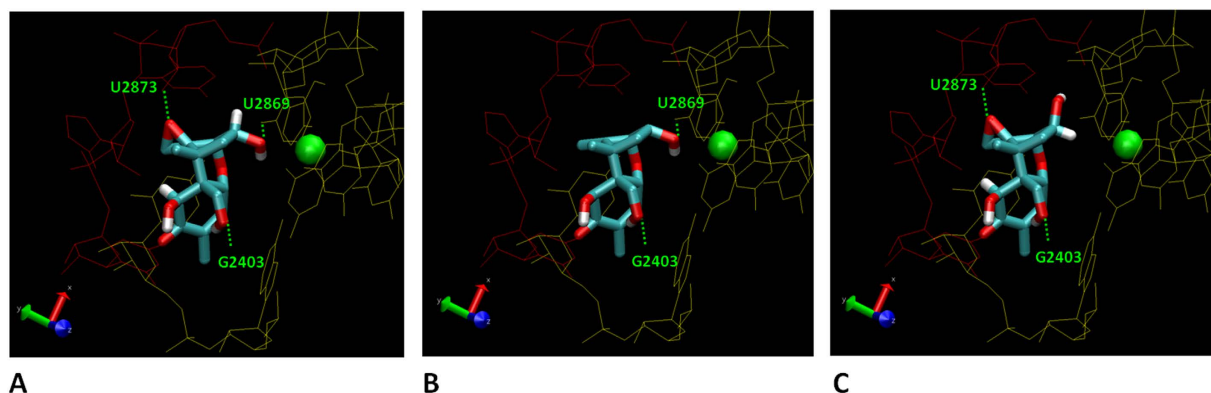


Figure 5. Interaction between the Ribosome 60S PTC subunit binding site and deepoxy-DON, 3-epi-DON or DON. Both sides of A site of the yeast ribosome 60S PTC subunit are colored in red and yellow respectively. Hydrogen and oxygen atoms are represented in white and red respectively. (Panel A): detailed views of the co-crystal (4UJX) of DON inside the A-site. (Panel B): detailed view of deepoxy-DON modeling inside the A-site. (Panel C): detailed views of 3-epi-DON modeling inside the A-site. The magnesium atom inside the A-site pocket has been pointed out in green.

hydrogen of the guanine base G2403) could be involved in the interaction of DON with the ribosome. It would be of interest to establish whether this hydrogen bond is necessary for the toxicity of DON. Unfortunately we were not able to identify a proper DON metabolite or another fusariotoxin metabolite to confirm the involvement of this hydrogen bond in the structure-toxicity relationship. A more thorough analysis, with additional trichothecenes would be needed to fully determine the molecular basis of toxicity.

In conclusion, the present study confirms that the toxicity of DON is not only linked to the epoxy group but is also influenced by the C3 group^{16,19,46}. It demonstrates that microbial biotransformation of DON into deepoxy-DON or 3-epi-DON decreases the intestinal toxicity of this mycotoxin. The underlying metabolism causes decreased affinity of the metabolites to the ribosome and the lack of MAPKinases activation. These data significantly increase the current knowledge of intestinal toxicity of DON, deepoxy-DON and 3-epi-DON and contribute to the evaluation of the effectiveness of the microbial biotransformation strategies in the fight against mycotoxins.

Methods

Toxins. Purified DON was purchased from Sigma-Aldrich (St Louis, MO, USA). Deepoxy-DON was obtained by transformation of crystalline DON (Romer Labs, Tulln, Austria), dissolved in medium 10^{47} at a concentration of 2 mg/ml, by inoculation with BBSH 797, *Gen. nov. sp. nov. of family Coriobacteriaceae* in sterile medium, at 37 °C for six days. Biotransformation of DON to deepoxy-DON was confirmed by LC-MS/MS, and deepoxy-DON was purified by solid phase extraction and preparative HPLC⁴⁸. The purity of the deepoxy-DON preparation was 99%, based on chromatograms recorded at 220 nm. The identity of deepoxy-DON was confirmed by comparison of enhanced product ion spectra of the preparation used in the present study with a reference standard (Romer Labs, Tulln, Austria) recorded on a 4000 QTrap mass spectrometer at a collision energy of 30 eV (Supplementary Figure S2).

3-epi-DON was produced by microbial transformation of DON²¹. Briefly, DON was co-incubated with the bacterial strain, *Devosia mutans* 17-2-E-8, in corn meal broth medium at 28 °C for 48 h. High-speed counter-current chromatography (HSCCC) and preparative high performance liquid chromatography (prep-LC) were applied to separate 3-epi-DON. The obtained product was analyzed by liquid chromatography (LC) and identified by congruent retention time and UV/Vis spectrum and mass spectrometric (MS) data. Nuclear magnetic resonance (NMR) experiments such as correlation spectroscopy (COSY), heteronuclear single quantum coherence (HSQC) and nuclear overhauser effect (NOE) were conducted for structural characterization of 3-epi-DON. Purification and structure identification of 3-epi-DON was already demonstrated in a previous publication²¹. The 3-epi-DON used in the experiment had a purity of 96.8%.

Toxins were dissolved in dimethyl sulfoxide (DMSO) (Sigma-Aldrich) and stored at −20 °C until use.

Caco-2 cell culture. Caco-2 cells (passages 99 - 106) obtained from the TC7 were cultured in 75-cm² culture flasks (Cellstar cell culture flasks, Sigma-Aldrich) in Dulbecco's Modified Eagle Medium enriched with glutamine (Gibco, Cergy-Pontoise, France), supplemented with 10% of heat inactivated fetal bovine serum, 0.5% of gentamycin (Eurobio, Courtaboeuf, France) and 1% of non-essential amino acids (Sigma-Aldrich). Cells were maintained at 37 °C in an atmosphere of 5% CO₂ and 90% relative humidity. The medium was changed every 2 days. Cells were passaged once a week. The partially confluent cell monolayers were trypsinized with Trypsin-EDTA (Eurobio).

Cell viability assay. Cell viability assay was performed with the CellTiter-Glo Luminescent Cell Viability Assay (Promega, Madison, USA) according to manufacturer's instruction. This test measures the quantity of ATP, proportional to the quantity of cells. Cells were seeded at the density of 1.56×10^5 cells/cm² in 96-well microtiter

plates. Cells were grown for 24 hours and exposed to DON, deepoxy-DON or 3-epi-DON, or corresponding concentrations of DMSO, for 48 hours. Luminescence was measured with a spectrophotometer (TECAN Infinite M200, Männedorf, Switzerland).

Trans-epithelial electrical resistant measurements. To assess the integrity of individual monolayers, trans-epithelial electrical resistance (TEER) was measured as already described^{49,50}. Cells (1.34×10^5 cells/cm²) were grown until differentiation on polyethylene terephthalate membrane inserts (surface area 0.3 cm², pore size 0.4 μm) in 24-well format (Becton Dickinson, Pont de Claix, France). The medium was changed every two days. Differentiated cells were exposed to 10 μM of diluent or toxins, DON, deepoxy-DON or 3-epi-DON. The culture medium in the apical side of differentiated cells in each well was replaced every two days with medium containing toxin. The TEER was measured for each well daily for 11 days using a Millicell-ERS Voltohmmeter (Millipore, Saint-Quentin-en-Yvelines, France). TEER values were expressed as % of initial values.

Oxygen consumption measurements. The acute effect of toxins on oxygen consumption of Caco-2 cells was assessed using an XF24 extracellular flux analyzer (Seahorse Bioscience, North Billerica, USA). The procedure was performed according to the manufacturer's instructions. Briefly, cells were cultured in XF24 cell culture microplates at 1.5×10^4 cells per well and maintained as described above. Oxygen consumption rates (OCR) were measured in proliferated Caco-2 cells in non-buffered DMEM (Seahorse Bioscience) supplemented with 10 mM glucose, 2 mM sodium pyruvate (Sigma-Aldrich) and 2 mM glutamine (Eurobio) and adjusted to pH 7.4. OCR was monitored every 20 minutes before (basal level) and after injection of diluent or toxins (10 μM). OCR values from each well were normalized against viable cell counts (calculated with a Malassez cell) and expressed as a percentage of the baseline value.

Intestinal jejunal explants. Jejunal explants were obtained from 5 week old crossbred castrated male piglets as described previously²⁴. The experiment was conducted under the guidelines of the French Ministry of Agriculture for animal research. All animal experimentation procedures were approved by the Ethics committee of Pharmacology-Toxicology of Toulouse-Midi-Pyrénées in animal experimentation (Toxcométhique), N°: TOXCOM/0017/IO PP, in accordance with the European Directive on the protection of animals used for scientific purposes (Directive 2010/63/EU). Two authors (I.P.O. and A.P.) have an official agreement with the French Veterinary Services permitting animal experimentation. Explants were treated for 4 hours at 39 °C with 10 μM of toxins (DON, deepoxy-DON or 3-epi-DON) or diluent (DMSO) in complete medium. After incubation, treated explants were fixed in 10% formalin (Sigma-Aldrich) for histological analysis or stored at -80 °C for RNA extraction.

Histological assessment. Explants fixed with 10% formalin for 24 hours were dehydrated and embedded in paraffin wax (Labonord, Templemars, France) according to standard histological procedures. Sections of 5 μm were stained with haematoxylin and eosin (Sigma-Aldrich) for histopathological assessment. Histological findings were scored based on histological changes and the severity of lesions as previously described²⁴.

Gene expression analysis of explants by RT-qPCR. For the gene expression analysis, total RNAs were extracted in lysing matrix D tubes (MP Biomedicals, Illkirch, France) containing guanidine thiocyanate-acid phenol (Eurobio). The quality of these RNA was assessed (Agilent RNA 6000 Nano Kit Quick, Agilent Bioanalyzer 2100); the mean RNA Integrity Number (RIN) of these mRNA preparations was 6.32 ± 0.83 .

Reverse transcription and RT-qPCR steps were performed as already described^{51,52} with previously published primers (Supplementary Table S1)²³. Amplification efficiency and initial fluorescence were determined by the Δ Ct method. Obtained values were normalized using two reference genes, ribosomal protein L32 (RPL32) and cyclophilin A (CycloA). Gene expression levels of treated explants were expressed relative to the mean of the control explants.

Gene expression analysis by microarray. The microarray GPL16524 (Agilent technology, 8 × 60 K) used in this experiment consisted of 43,603 spots derived from the 44 K (V2:026440 design) Agilent porcine specific microarray. This was enhanced with 9,532 genes from adipose tissue, 3,776 genes from the immune system and 3,768 genes from skeletal muscle^{23,53}. For each sample, Cyanine-3 (Cy3) labeled cRNA was prepared from 200 μg of total RNA using the One-Color Quick Amp Labeling kit (Agilent) according to the manufacturer's instructions, followed by Agencourt RNAClean XP (Agencourt Bioscience Corporation, Beverly, Massachusetts). About 600 ng of Cy3-labelled cRNA were hybridized on SurePrint G3 Porcine GE microarray (8 × 60 K) following the manufacturer's instructions. Slides were scanned immediately, after washing on an Agilent G2505C Microarray Scanner with Agilent Scan Control A.8.5.1 software. All experimental details are available in the Gene Expression Omnibus (GEO) database under accession GSE66918 (<http://www.ncbi.nlm.nih.gov/geo/query/acc.cgi?token=olixoose&dvmdnqr&acc=GSE66918>).

The differentially expressed (DE) genes (adjusted p-value ≤ 0.05) were hierarchically clustered and visualized in heat maps. Functional analysis of DE genes was performed using the Ingenuity pathway Analysis tool (IPA, <http://www.ingenuity.com>) to identify pathways and processes affected by toxins.

Immunoblotting. Expression of the phosphorylated MAPK p38 and JNK (Jun amino-terminal kinases) was assessed on differentiated Caco-2 cells and jejunal explants by immunoblotting as previously described^{49,54}. Cells differentiated on 24-well inserts or explants were treated with 10 μM of diluent (DMSO) or toxins, DON, deepoxy-DON or 3-epi-DON for 1 hour. Proteins were extracted, quantified and a total of 15 μg of protein was separated by SDS-PAGE. The membranes were probed with rabbit antibodies (Cell Signaling Technology, Danvers, USA) specific for: phospho-SPAK/JNK or phospho-p38 diluted at 1:500 or GAPDH diluted at 1:1000.

After washing, the membranes were incubated with 1:10,000 CFTM770 goat anti-rabbit IgG (Biotium, Hayward, USA) for the detection. Antibody detection was performed using an Odyssey Infrared Imaging Scanner (Li-Cor Science Tec, les Ulis, France) with the 770 nm channel. The expression of the proteins was estimated after normalization with GAPDH signal.

Molecular modeling. The yeast 80S ribosome X-ray structure, determined at a resolution of 3.3 Å (PDB code 4U53¹³), was used in all docking calculation. The whole chain A of the ribosome peptidyl transferase center was taken into account. The atomic coordinates of the PDB file were used for docking calculations using NAMD under VMD1.9⁵⁵. VMD was used as visualization tools for various tasks (alignments, ligands location). The molecular structures of deepoxy-DON and 3-epi-DON were built using molefacture from the DON structure included in PDB-file 4U53, after adding hydrogen and after verification of the chirality and the type of each atoms. Ligand structures were minimized by NAMD using AMBER force field topology and parameter files. Molecular docking experiments of deepoxy-DON and 3-epi-DON were done in VMD based on the superposition of the carbon backbone of DON. To relax structures and to evaluate the interaction of hydrogen bonds between ribosome and ligand, a semi-rigid energy minimization was calculated by NAMD using AMBER topology and parameter files with a fixed ribosome structure and a flexible structure for the ligand. Associated to PDB-file 4U53 of DON, PDB-file 4U53 including structure of deepoxy-DON and 3-epi-DON are available in Supplementary Data (SupplementaryData_S1_4U53wDON, Supplementary Data_S2_4U53wdepoxyDON and SupplementaryData_S3_4U53w3EpiDON).

Statistical analysis. Data are expressed as a mean ± SEM of values. The results were analyzed using the Fisher test on equality of variances, one-way ANOVA and Bonferroni as a test post-hoc; p-values < 0.05 were considered significant. Microarray data from Feature Extraction software was analyzed with R using Bioconductor packages and the limma lmFit function as previously described²³. Probes with adjusted p-value ≤ 0.05 were considered differentially expressed between treated and control conditions. Hierarchical clustering was applied to the samples and the probes using 1-Pearson correlation coefficient as distance and Ward's criterion for agglomeration.

References

- Bennett, J. W. & Klich, M. Mycotoxins. *Clin Microbiol Rev* **16**, 497 (2003).
- Frisvad, J. C., Nielsen, K. F. & Samson, R. A. Recommendations concerning the chronic problem of misidentification of mycotoxigenic fungi associated with foods and feeds. *Adv Exp Med Biol* **571**, 33 (2006).
- Awad, W. A., Ghareeb, K., Bohm, J. & Zentek, J. Decontamination and detoxification strategies for the Fusarium mycotoxin deoxynivalenol in animal feed and the effectiveness of microbial biodegradation. *Food Addit Contam Part A Chem Anal Control Expo Risk Assess* **27**, 510 (2010).
- EFSA. Deoxynivalenol in food and feed: occurrence and exposure. *EFSA Journal* **11**, 3379 (2013).
- CAST, Mycotoxins: Risks in Plant, Animal, and Human Systems. *Council for Agricultural Science and Technology-Potential economic costs of mycotoxins in United States* Task Force Rep. 138 (Iowa, USA), 136 (2003).
- Pestka, J. J. Deoxynivalenol: mechanisms of action, human exposure, and toxicological relevance. *Arch Toxicol* **84**, 663 (2010).
- Maresca, M. From the gut to the brain: journey and pathophysiological effects of the food-associated mycotoxin Deoxynivalenol. *Toxins* **5**, 784 (2013).
- Pinton, P. & Oswald, I. P. Effect of deoxynivalenol and other Type B trichothecenes on the intestine: a review. *Toxins* **6**, 1615 (2014).
- Cano, P. M. *et al.* Deoxynivalenol as a new factor in the persistence of intestinal inflammatory diseases: an emerging hypothesis through possible modulation of Th17-mediated response. *PLoS One* **8**, e53647 (2013).
- Vandenbroucke, V. *et al.* The mycotoxin deoxynivalenol potentiates intestinal inflammation by salmonella typhimurium in porcine ileal loops. *PLoS One* **6**, e23871 (2011).
- Shifrin, V. I. & Anderson, P. Trichothecene mycotoxins trigger a ribotoxic stress response that activates c-Jun N-terminal kinase and p38 mitogen-activated protein kinase and induces apoptosis. *J Biol Chem* **274**, 13985 (1999).
- Pestka, J. J., Zhou, H. R., Moon, Y. & Chung, Y. J. Cellular and molecular mechanisms for immune modulation by deoxynivalenol and other trichothecenes: unraveling a paradox. *Toxicol Lett* **153**, 61 (2004).
- Garreau de Loubresse, N. *et al.* Structural basis for the inhibition of the eukaryotic ribosome. *Nature* **513**, 517 (2014).
- Pestka, J. J. Deoxynivalenol-induced proinflammatory gene expression: mechanisms and pathological sequelae. *Toxins* **2**, 1300 (2010).
- Zhou, T., He, J. & Gong, J. Microbial transformation of trichothecene mycotoxins. *World Mycotoxin J* **1**, 23 (2008).
- Sundstol Eriksen, G., Pettersson, H. & Lundh, T. Comparative cytotoxicity of deoxynivalenol, nivalenol, their acetylated derivatives and de-epoxy metabolites. *Food Chem Toxicol* **42**, 619 (2004).
- Schatzmayr, G. *et al.* Microbiologicals for deactivating mycotoxins. *Mol Nutr Food Res* **50**, 543 (2006).
- Grenier, B. *et al.* Biotransformation approaches to alleviate the effects induced by fusarium mycotoxins in swine. *J Agric Food Chem* **61**, 6711 (2013).
- Karlovsky, P. Biological detoxification of the mycotoxin deoxynivalenol and its use in genetically engineered crops and feed additives. *Appl Microbiol Biotechnol* **91**, 491 (2011).
- Berthiller, F. *et al.* Masked mycotoxins: a review. *Mol Nutr Food Res* **57**, 165 (2013).
- He, J. W. *et al.* An epimer of deoxynivalenol: purification and structure identification of 3-epi-deoxynivalenol. *Food Addit Contam Part A Chem Anal Control Expo Risk Assess* **32**, 1523 (2015).
- He, J. W. *et al.* Toxicology of 3-epi-deoxynivalenol, a deoxynivalenol-transformation product by *Devosia* mutants 17-2-E-8. *Food Chem Toxicol* **84**, 250 (2015).
- Pierron, A. *et al.* Intestinal toxicity of the masked mycotoxin deoxynivalenol-3-beta-D-glucoside. *Arch Toxicol in press* (2016).
- Lucioli, J. *et al.* The food contaminant deoxynivalenol activates the mitogen activated protein kinases in the intestine: Interest of *ex vivo* models as an alternative to *in vivo* experiments. *Toxicol* **66**, 31 (2013).
- Swanson, S. P., Rood, H. D., Jr., Behrens, J. C. & Sanders, P. E. Preparation and characterization of the deepoxy trichothecenes: deepoxy HT-2, deepoxy T-2 triol, deepoxy T-2 tetraol, deepoxy 15-monoacetoxyscirpenol, and deepoxy scirpentriol. *Appl Environ Microbiol* **53**, 2821 (1987).
- Li, X. Z. *et al.* Efficacy of detoxification of deoxynivalenol-contaminated corn by *Bacillus* sp. LS100 in reducing the adverse effects of the mycotoxin on swine growth performance. *Food Addit Contam Part A Chem Anal Control Expo Risk Assess* **28**, 894 (2011).
- He, P., Young, L. G. & Forsberg, C. Microbially detoxified vomitoxin-contaminated corn for young pigs. *J Anim Sci* **71**, 963 (1993).

28. Alassane-Kpembi, I. *et al.* New insights into mycotoxin mixtures: The toxicity of low doses of Type B trichothecenes on intestinal epithelial cells is synergistic. *Toxicol Appl Pharmacol* **272**, 191 (2013).
29. Akbari, P. *et al.* Deoxynivalenol: a trigger for intestinal integrity breakdown. *FASEB J* **28**, 2414 (2014).
30. Bin-Umer, M. A. *et al.* Elimination of damaged mitochondria through mitophagy reduces mitochondrial oxidative stress and increases tolerance to trichothecenes. *Proc Natl Acad Sci USA* **111**, 11798 (2014).
31. Nejdfors, P., Ekelund, M., Jeppsson, B. & Westrom, B. R. Mucosal *in vitro* permeability in the intestinal tract of the pig, the rat, and man: species- and region-related differences. *Scand J Gastroenterol* **35**, 501 (2000).
32. van Kol, S. W., Hendriksen, P. J., van Loveren, H. & Peijnenburg, A. The effects of deoxynivalenol on gene expression in the murine thymus. *Toxicol Appl Pharmacol* **250**, 299 (2011).
33. Katika, M. R. *et al.* Transcriptome analysis of the human T lymphocyte cell line Jurkat and human peripheral blood mononuclear cells exposed to deoxynivalenol (DON): New mechanistic insights. *Toxicol Appl Pharmacol* **264**, 51 (2012).
34. Mishra, Sakshi, Dwivedi, Premendra D., Pandey, Haushila P. & Das, Mukul Role of oxidative stress in Deoxynivalenol induced toxicity. *Food Chem Toxicol* **72**, 20 (2014).
35. Shen, Y. *et al.* ER stress differentially regulates the stabilities of ERAD ubiquitin ligases and their substrates. *Biochem Biophys Res Commun* **352**, 919 (2007).
36. Osman, A. M. *et al.* Protein expression profiling of mouse thymoma cells upon exposure to the trichothecene deoxynivalenol (DON): implications for its mechanism of action. *J Immunotoxicol* **7**, 147 (2010).
37. Kumar, A. *et al.* Mammalian proapoptotic factor ChaC1 and its homologues function as gamma-glutamyl cyclotransferases acting specifically on glutathione. *EMBO Rep* **13**, 1095 (2012).
38. Vasatkova, A. *et al.* Changes in metallothionein level in rat hepatic tissue after administration of natural mouldy wheat. *Int J Mol Sci* **10**, 1138 (2009).
39. Bookstein, C. *et al.* Tissue distribution of Na⁺/H⁺ exchanger isoforms NHE2 and NHE4 in rat intestine and kidney. *Am J Physiol* **273**, C1496 (1997).
40. Smith, D. E., Clemenccon, B. & Hediger, M. A. Proton-coupled oligopeptide transporter family SLC15: physiological, pharmacological and pathological implications. *Mol Aspects Med* **34**, 323 (2013).
41. Dietrich, B., Neuenschwander, S., Bucher, B. & Wenk, C. Fusarium mycotoxin-contaminated wheat containing deoxynivalenol alters the gene expression in the liver and the jejunum of broilers. *Animal* **6**, 278 (2012).
42. Maresca, M., Mahfoud, R., Garmy, N. & Fantini, J. The mycotoxin deoxynivalenol affects nutrient absorption in human intestinal epithelial cells. *J Nutr* **132**, 2723 (2002).
43. Videmann, B., Tep, J., Cavret, S. & Lecoeur, S., Epithelial transport of deoxynivalenol: involvement of human P-glycoprotein (ABCB1) and multidrug resistance-associated protein 2 (ABCC2). *Food Chem Toxicol* **45**, 1938 (2007).
44. Nakamura, M. T., Yudell, B. E. & Loor, J. J. Regulation of energy metabolism by long-chain fatty acids. *Prog Lipid Res* **53**, 124 (2014).
45. Sergent, T. *et al.* Deoxynivalenol transport across human intestinal Caco-2 cells and its effects on cellular metabolism at realistic intestinal concentrations. *Toxicol Lett* **164**, 167 (2006).
46. Sato, I. & Ueno, Y. Comparative toxicities of trichothecenes. In Rodricks, J. V., Hesseltnie, C. W., Mehlman, M. A. (eds) *Mycotoxins in human and animal health* Pathotox Publishers, Park Forest South, IL, 295 (1977).
47. Caldwell, D. R. & Bryant, M. P. Medium without rumen fluid for nonselective enumeration and isolation of rumen bacteria. *Appl Microbiol* **14**, 794 (1966).
48. Schwartz-Zimmermann, H. E. *et al.* Deoxynivalenol (DON) sulfonates as major DON metabolites in rats: from identification to biomarker method development, validation and application. *Anal Bioanal Chem* **406**(30), 7911 (2014).
49. Pinton, P. *et al.* Toxicity of deoxynivalenol and its acetylated derivatives on the intestine: differential effects on morphology, barrier function, tight junction proteins, and mitogen-activated protein kinases. *Toxicol Sci* **130**, 180 (2012).
50. Loiseau N. *et al.* Fumonisin B₁ exposure and its selective effect on porcine jejunal segment: sphingolipids, glycolipids and transepithelial-passage disturbance. *Biochem. Pharmacol.* **74**, 144 (2007).
51. Halloy, D. J., Gustin, P. G., Bouhet, S. & Oswald, I. P. Oral exposure to culture material extract containing fumonisins predisposes swine to the development of pneumonitis caused by *Pasteurella multocida*. *Toxicology* **213**, 34 (2005).
52. Gourbeyre, P. *et al.* Pattern recognition receptors in the gut: analysis of their expression along the intestinal tract and the crypt/villus axis. *Physiol Rep* **3**(2), e12225 (2015).
53. Gao, Y. *et al.* Transcriptome analysis of porcine PBMC after stimulation by LPS or PMA/ionomycin using an expression array targeting the pig immune response. *BMC genomic* **11**, 292 (2010).
54. Meissonnier G. M. *et al.* Subclinical doses of T-2 toxin impair acquired immune response and liver cytochrome P450 in pigs. *Toxicology* **247**, 46 (2008).
55. Humphrey, W., Dalke, A. & Schulten, K. VMD: visual molecular dynamics. *J Mol Graph* **14**, 33 (1996).

Acknowledgements

The authors are grateful to A.M. Cossalter, J. Laffitte and P. Pinton (INRA Toxalim) for sample collection and western-blot experiments. The authors thank Drs L. Huc (INRA, Toxalim), F. Smih-Rouet and M. Barutaut (I2MC INSERM UMR 1048) for Bioenergetic measurements and H.E. Schwartz-Zimmermann for preparation and characterization of deepoxy-DON. Thanks are also due to C.A. Moll for language editing. A. Pierron and L.S. Murate were supported by fellowships from CIFRE (2012/0572, jointly financed by the BIOMIN Holding GmbH, Association Nationale de la Recherche Technique and INRA) and CAPES (Brazil) respectively.

Author Contributions

A.P. and S.M. performed *in vitro*, *ex vivo*, Q-PCR experiments and IPA analysis. A.P., F.L.B. and L.S.M. performed histological analysis. L.S.M. performed western analysis and helped with *in vitro* experiments. Y.L. and N.L. performed microarray analysis and *in silico* modeling respectively. W.-D.M. and G.S. characterized, purified and provided the deepoxy-DON, J.W.H. and T.Z. characterized, purified and provided the 3-epi-DON. I.P.O., G.S. and W.-D.M. provided conception and design of research. A.P., S.M. and I.P.O. wrote the manuscript.

Additional Information

Supplementary information accompanies this paper at <http://www.nature.com/srep>

Competing financial interests: The authors declare no competing financial interests.

How to cite this article: Pierron, A. *et al.* Microbial biotransformation of DON: molecular basis for reduced toxicity. *Sci. Rep.* **6**, 29105; doi: 10.1038/srep29105 (2016).



This work is licensed under a Creative Commons Attribution 4.0 International License. The images or other third party material in this article are included in the article's Creative Commons license, unless indicated otherwise in the credit line; if the material is not included under the Creative Commons license, users will need to obtain permission from the license holder to reproduce the material. To view a copy of this license, visit <http://creativecommons.org/licenses/by/4.0/>